ACS Macro Letters

Letter

pubs.acs.org/macroletters

From Hyperbranched Polymer to Nanoscale CMP (NCMP): Improved Microscopic Porosity, Enhanced Light Harvesting, and Enabled Solution Processing into White-Emitting Dye@NCMP Films

Peng Zhang,† Keyi Wu,† Jia Guo,* and Changchun Wang

State Key Laboratory of Molecular Engineering of Polymers, Department of Macromolecular Science, Fudan University, Shanghai 200433, People's Republic of China

Supporting Information

ABSTRACT: A two-step polymerization combining miniemulsion and solvothermal techniques was applied to synthesize tetraphenylethene-based nanoscale conjugated microporous polymers (TPE-NCMP), which simultaneously possessed a large surface area (1214 m^2/g) and a high aggregation-induced florescence quantum yield (58%). Immobilization of Nile Red within micropores of TPE-NCMPs constructed a light-harvesting composite with characteristics of intense photons acquisition and efficient energy migration. Homogenous NCMP-based films were fabricated by blending the dye-doped TPE-NCMPs with PVA. The fluorescence emission could be flexibly tuned by varying the dosage of dyes over the whole visible spectrum including a pure white light.

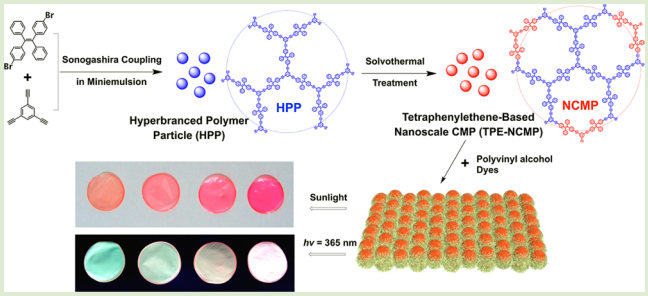

The chemistry of conjugated microporous polymers (CMPs) has evolved rapidly in recent years.[1−9] Extensive research has paid particular attention to the storage and separation of gases by virtue of the outstanding CMP microporosity.[10−16] Meanwhile, recent reports have also demonstrated that diverse functional modules, such as porphyrins, phthalocyanines, perylene bisimides, naphthalene, pyrene, and so on, are enabled to constitute CMPs for a broad range of applications, including heterogeneous catalysis,[17−19] light harvesting/emission,[20,21] chemical sensing,[6,22] and supercapacitive storage.[23,24] Further progress to date, however, remains greatly challenged because the stiff CMP networks cannot be well dispersed in common solvents resulting in a large limitation of processing and assembling into versatile forms like spheres, fibers, films, or any other desired shapes. To circumvent the issue, Cooper and co-workers presented the two-step approach to constituting the dendrimer-like soluble CMPs, but they more resemble hyperbranched polymers rather than inherent interconnected CMP networks.[25] Novel synthetic techniques have also been pursued to directly prepare CMP membranes on substrates. An electrochemical method was employed to fabricate CMP films for use in electronic devices.[8,26,27] However, the electrochemically synthesized CMPs are difficult to confirm the definite structural natures because the yield is not much. The third method is based on a miniemulsion technique.[28−31] Dispersible and discrete nanoscale CMPs (NCMPs) have been prepared by this way and the morphologies and sizes could be modulated in the nanodroplets of miniemulsion. In contrast to the dendrimer-like soluble CMP, NCMPs retain the permanent intrinsic micropores without change upon removal of solvent molecules. Thus, the development of NCMPs has more possibilities to realize versatility and applicability in comparison to those synthesized by the other ways. However, on account of the emulsion stabilization, the synthesis of NCMPs needs a low temperature, a nonpolar solvent as droplet phase and a short reaction time; thereby, the resulting surface areas are impaired and the pore size distributions are flawed due to the low polymerization degree. In addition, since many conjugated molecules tend to dissolve in polar solvents, they are plagued by the poor solubility in the oil-phase droplets of miniemulsion. Thus, exploration of functional NCMPs has remained challenged over recent years.

In this report, we proposed a two-step method to endow NCMPs with the improved microporosity, controlled sizes and morphologies, dispersibility and functionality. As illustrated in Scheme 1, 1,2-bis(4-bromophenyl)-1,2-diphenylethene and 1,3,5-triethynyl benzene are subjected to the Pd-catalyzed Sonogashira coupling in a routine toluene-in-water miniemulsion. The primary particles are hyperbranched with a certain form and size, but without permanent micropores that are given by rigid CMP scaffolds. To convert them into NCMPs, the miniemulsion solution is transferred into a Teflon-lined stainless steel autoclave, and the reaction is continued at elevated temperatures and high vapor pressures. It is expected that the hyperbranched polymer particles (HPPs) could be reacted further with the rest of monomers or oligmeric chains by the Sonogashira cross-coupling reaction, thus, resulting in a

Received: September 3, 2014
Accepted: October 14, 2014
Published: October 16, 2014

ACS Publications © 2014 American Chemical Society

Scheme 1. Illustration of Preparation of NCMP from HPP by Combining Miniemulsion and Solvothermal Techniques

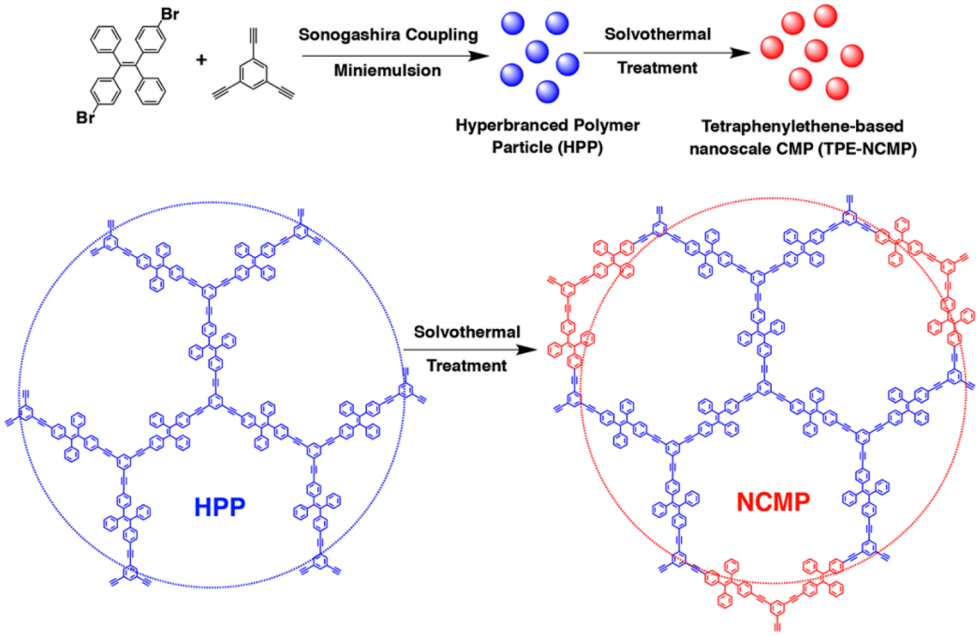

network-structured NCMP. This two-step method not only maintains uniformity and regularity of NCMPs in size and morphology, but also gives rise to a significantly enhanced intrinsic porosity, opening up an applicable avenue in a controlled synthesis of high-quality NCMPs.

To elucidate the feasibility of synthetic method, poly(aryleneethynylene)-based NCMP-1 was first synthesized by the two-step process and compared with the reported CMP-1[1] and CNPC,[29] both of which have the identical compositions but are prepared in toluene solution and in toluene-in-water miniemulsion, respectively. For NCMP-1, the first reaction stage occurred in the toluene-in-water miniemulsion with standard Sonogashira catalysts (Et_3N, CuI, and $Pd(PPh_3)_4$) at 70 °C for 3 h; then the solution was transferred into a 50 mL autoclave and was subjected to the severe conditions for further polymerization. Prior to the solvothermal treatment, HPP-1 extracted out of the miniemulsion could be partially dissolved in THF. SEC analysis revealed that THF soluble fraction had number-average molar mass (M_n) of 2665 and polydispersity of 1.60 (Figure S1 in Supporting Information (SI)). This indicates that the soluble fraction is hyperbranched in architecture, and the insoluble fraction is possibly cross-linked with a higher molecular weight. For the solvothermally treated NCMP-1, TEM images (Figure S2 in SI) show that the resulting particles do not collapse under harsh conditions, but keep the spherical morphology intact and the particle size are narrowly distributed around 100 nm. The porosity of NCMP-1 estimated by N_2 adsorption measurement was pronouncedly enhanced. As shown in Table S1 (SI), HPP-1 displays the surface area of as low as 43 m^2/g, indicating that the hyperbranched structure with flexible bending or rotating chains is incapable of affording permanent micropores. The unreacted monomers or oligmers are encapsulated within HPP-1 in the droplets and, thus, the further reaction is allowed in the second step. As the solvothermal treatment proceeded at elevated temperatures for 12 h, there is evidence that the BET surface areas and pore volumes were both greatly enhanced. The optimized results were obtained at 150 °C, giving a surface area of 1089 m^2/g and a pore volume of 1.13 cm^3/g. Meanwhile, the N_2 sorption isotherms (Figure S3 in SI) showed the characteristic of micropore adsorption, and the micropore surface area estimated by the analysis of *t-plot* method was up to 796 m^2/g. In contrast to the reported CMP-1 (834 m^2/g) and CNPC (421 m^2/g), NCMP-1 prepared by the two-step process is superior in pore properties and also retain a controlled morphology and size.

CMPs have many unprecedented advantages in light harvesting and energy transduction as compared to the linear conjugated polymers.[21] Particularly, the dense light-adsorbing units on the periphery of networks can act as antenna to capture the photons, and the excitation energy transfer is channeled through the networks in the cooperative fashion. Triggered by the above finding, we expanded the scope of building blocks to constitute a novel photofunctional NCMP by the two-step strategy. Tetraphenylethene (TPE) is a typical aggregation-induced emission (AIE) chromophore,[32,33] which restricts the twisting of the peripheral phenyl groups and enhances the luminescence activity in the form of intermolecular aggregation. Jiang and co-workers employed the Yamamoto reaction to knit a CMP network using TPE units, whose four phenyl groups are all locked into the network skeletons and imposed on a planar conformation to achieve the enhanced luminescence emission, large π-electronic conjugation and promoted exciton migration.[34] However, how to create the nanosized TPE-CMP still remains greatly challenged as it has come to be known.

At initial trials, one-step miniemulsion polymerization was used to form TPE-NCMPs, but the solubility of monomers was very poor in toluene and the formed particles had no pores. Thus, following the miniemulsion reaction, the TPE-HPPs were further treated in a solvothermal way. TEM images display the particles synthesized using miniemulsion and two-step continuous routes, respectively (Figure 1). The resulting TPE-NCMPs (Figure 1b) have regular shape, are discretely distributed, and have an average diameter of approximately 100 nm. In comparison with TPE-HPPs (Figure 1a), the dimension, size distribution, and morphology of the TPE-NCMPs are all well maintained, without influence of the harsh

dx.doi.org/10.1021/mz5005508 | *ACS Macro Lett.* 2014, 3, 1139−1144

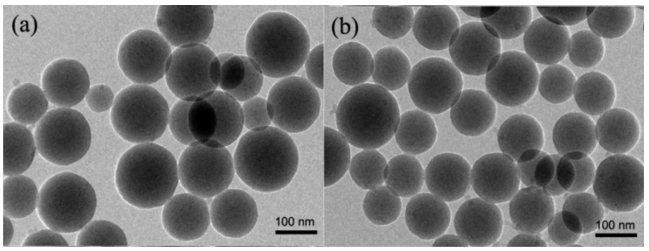

Figure 1. HR TEM images of TPE-HPP (a) and TPE-NCMP (b) microspheres.

reaction conditions. Dynamic light scattering was employed to examine the dispersibility of particles in aqueous solution. Figure S4 (SI) shows the histograms of the hydrodynamic diameter distributions for TPE-HPPs and TPE-NCMPs stabilized with surfactants. As compared to the forms in the dry state (shown in the TEM image), they both gave the larger particle sizes of ~340 nm. It is probably because the residual toluene is present to cause the particles swelling in solution. The molecular composition was verified by solid-state ^{13}C cross-polarization magic-angle spinning (CP/MAS) NMR (Figure 2). In addition to the aromatic carbons from the

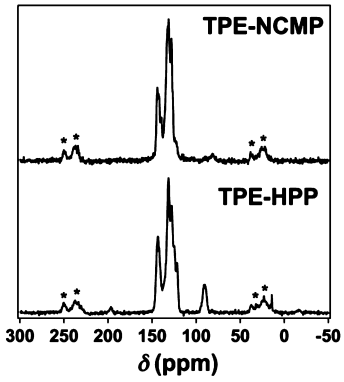

Figure 2. Solid-state ^{13}C CP/MAS NMR spectra of TPE-NCMP and TPE-HPP at a CP contact time of 2 ms and a MAS rate of 12 kHz. Signals with * symbols are side peaks.

TPE components, it is found that the terminal acetylene of TPE-HPP resonates at $\delta = 90.6$, which almost disappears in the spectrum of TPE-NCMP. This indicates that the reaction is almost completed after the solvothermal treatment. Therefore, the cross-linking degree could be significantly improved to construct intrinsic microporous architectures. Although the side reactions generally occur in the Sonogashira coupling, as reported for the other known alkyne-bridged CMPs,[9] the trace impurities rarely affect pore properties.

The solvothermal temperature and time were optimized to improve surface areas and pore volumes of TPE-NCMPs. As shown in Table 1, the polymerization temperature was varied from 120 to 150 °C, and the reaction time was extended from 6 to 24 h. All of the synthesized TPE-NCMPs were examined by N_2 adsorption at 77 K and gave the corresponding gas sorption isotherms, as exhibited in Figure S5 (SI). According to IUPAC classification for the N_2 sorption isotherms, TPE-NCMP-3 and TPE-NCMP-4 are both of micropore characteristic, and TPE-NCMP-1 and TPE-NCMP-2 are equally mesoporous. In sharp contrast, TPE-HPP has a lower gas adsorption, and a hysteresis loop is present at high relative pressures indicating that the

Table 1. Pore Parameters of a Series of TPE-NCMPs Characterized by N_2 Adsorption at 77 K

material	T (°C)	time (h)	S_{BET}[a] (m^2/g)	V_{tot}[b] (cm^3/g)
TPE-HPP			30	0.05
TPE-NCMP-1	120	6	176	0.33
TPE-NCMP-2	150	6	459	0.38
TPE-NCMP-3	150	12	761	0.46
TPE-NCMP-4	150	24	1214	0.52

[a]Surface areas are calculated from the N_2 adsorption isotherms using the Brunauer–Emmett–Teller (BET) method. [b]Total pore volume at $P/P_0 = 0.99$.

accumulation pores are dominated. Using the Brunauer–Emmett–Teller (BET) model, the total pore volumes and surface areas were calculated and compiled in Table 1. TPE-HPP has a surface area of 30 m^2/g and a pore volume of 0.05 cm^3/g, proving that the hyperbranched structure is not rigid enough to support the voids within skeletons when the filling solvent molecules were extracted out. Upon the solvothermal treatment for 6 h at 120 °C, the BET surface area of TPE-NCMP-1 increases to 176 m^2/g, and the pore volume is up to 0.33 cm^3/g. When the reaction proceeded at 150 °C for 24 h, the BET surface area is dramatically improved up to 1214 m^2/g, and the pore volume is 0.52 cm^3/g. The pore size distributions of TPE-NCMPs were calculated using the Barrett–Joyner–Halenda (BJH) model for mesoporous TPE-NCMPs and the nonlocal density functional theory (NLDFT) model for microporous TPE-NCMPs, respectively. As shown in Figure S6 (SI), TPE-NCMP-1 and TPE-NCMP-2 both have flawed pore size distributions in the mesopore region, which are centered at ~6.2 and ~3.7 nm, respectively. We assume that the structural defects are originated from the low polymerization degree and the interpenetrating polymer chains. For the TPE-NCMP-3 and TPE-NCMP-4, both have typical micropores. The prevailing pore sizes are centered at 1.3 nm.

Thermal stability of TPE-NCMPs was assessed by thermal gravimetric analysis (Figure S7 in SI). In comparison to TPE-HPPs, the decomposing temperatures of TPE-NCMPs are slightly shifted to high temperatures as the solvothermal treatment is extended. TPE-NCMP-2 has the thermal tolerance under an air atmosphere but is worse than TPE-NCMP-4 both in decomposing temperature and mass loss rate. All these demonstrate again that the increasing cross-linking degree of polymer networks is beneficial to improve the structural stability.

In light of the AIE effect from TPE units, TPE-NCMPs were dispersed in a mixture of THF and water (1/9, v/v) that is conducive to restrain the twisting of phenyl rings of TPE units, and the optical properties were studied by using TPE and TPE-HPP as comparison. Figure 3a shows the normalized fluorescence emission spectra of TPE, TPE-HPP, and TPE-NCMP-4 excited at 340 nm. The corresponding maximum emission peaks are red-shifted from 480 to 500 to 520 nm, manifesting that the electronic conjugation of NCMPs becomes larger. Meanwhile, the fluorescence quantum yield of TPE-NCMP-4 was estimated in THF, THF–water mixture, and the solid state, respectively, in which THF is the good solvent to disperse NCMPs. The results were summarized in Table S2 (SI), and the AIE factor (α_{AIE}) that is defined by the ratio of Φ_{aggre} to Φ_{soln} was calculated as well. The Φ_{soln} values evaluated using Rhodamine 6G as standard are relatively low, reaching 0.04, 1.03, and 3.25% for TPE, TPE-HPP, and TPE-NCMP-4,

dx.doi.org/10.1021/mz5005508 | ACS Macro Lett. 2014, 3, 1139–1144

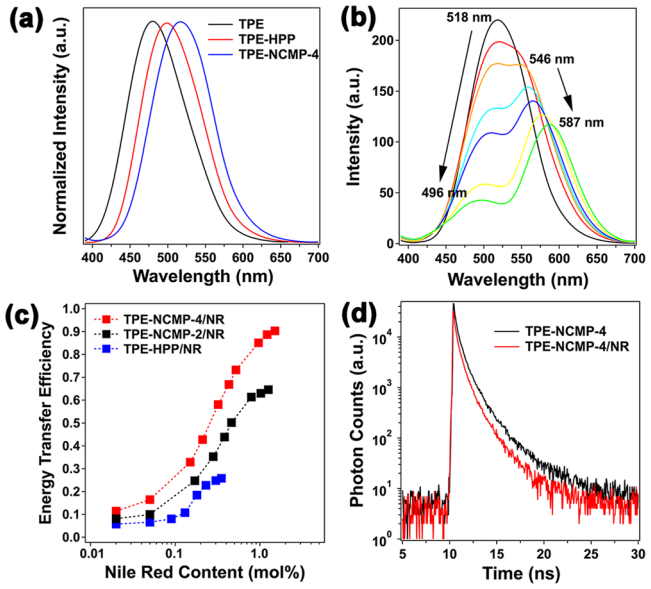

Figure 3. (a) Fluorescence emission spectra of TPE, TPE-HPP, and TPE-NCMP-4 in THF−H_2O mixture (1/9, v/v; λ_{ex} = 340 nm). (b) Fluorescence emission change of NR@TPE-NCMP-4 composites with 0−0.43 mol % NR (λ_{ex} = 380 nm). (c) Plot of quantum efficiency in energy transfer from TPE-NCMP to NR vs NR content. (d) Fluorescence decay profiles of TPE-NCMP-4 and NR@TPE-NCMP-4.

respectively. The quantum yield of TPE-NCMP-4 in THF is roughly 10× higher than that of TPE. It elucidates that the less rotatable phenyl rings of TPE blocks in NCMPs can limit the energy loss through the channel of nonradiative relaxation and hence increase the Φ_{soln} value dramatically. The Φ_{aggre} values of three samples are all considerably improved, proving the AIE effect occurring in 90% aqueous solution. Of three members, TPE-NCMP-4 affords the Φ_{aggre} of up to 42.1%, far better than those of TPE and TPE-HPP, but its α_{AIE} value (13.0) is the lowest. This implies that the TPE-knitting network structure is more effective to restrain the nonradiative energy yield in the aggregate state. The Φ_{solid} values of three samples were determined by a calibrated integrating sphere, and 58.0% Φ_{solid} for TPE-NCMP-4 was obtained, corroborating again their excellent AIE effect in the solid state.

In conjunction with the outstanding porosity of NCMPs, we pursued a light-harvesting composite prepared by loading dye molecules within micropores of TPE-NCMPs. Given the guest-to-host excitation energy transfer, a variety of dyes were screened, and Nile Red (NR) was applied in the study since we found it had a complementary fluorescent property relative to TPE-NCMPs. As measured in trial experiments, NR in ethanol solution exhibited a peak at 565 nm in the excitation spectrum and a peak at 620 nm in the emission spectrum (Figure S8 in SI). It hardly emitted fluorescence with excitation at 380 nm, but this wavelength could illuminate TPE-NCMPs. Thus, it is likely that if NR molecules are entrapped within TPE-NCMPs, the photonic energy would be harvested by numerous TPE units and transfer from NCMP skeletons to guest dyes.

Figure 3b shows the emission spectra of the assembled NR@TPE-NCMP in water upon excitation at 380 nm as the loading content of NR was varied. The emission at 518 nm from the TPE-NCMP-4 component is consecutively reduced with increase of the NR concentration, and it is also accompanied by the enhancement of emission in the window of 550−590 nm. Since the NR dye is not responded to the excitation light at 380 nm, the result sheds light on the fact that the photonic energy adsorbed by the TPE-NCMP is transferred to the NR without occurrence of a radiation-reabsorption process. Afterward, the quantitative study of the energy transfer process was conducted using the TPE-HPP (30 m^2/g), TPE-NCMP-2 (176 m^2/g), and TPE-NCMP-4 (1214 m^2/g), respectively, to examine the effect of porous structures on the energy transfer between NR and TPE units. Also, the energy-transfer efficiency (η_{ET}) was estimated from the quenching rate of TPE emission (=1 − $\Phi_F(c)/\Phi_F(0)$, where c is the NR concentration). As shown in Figure 3c, three curves are all evolved in a sigmoidal fashion and level off eventually, whereas the maximum η_{ET} values are greatly differentiated with each other. Roughly 90% of η_{ET} is obtained as 1.5 mol % of NR was embedded within TPE-NCMP-4. The low η_{ET} values are found for NR@TPE-NCMP-2 and NR@TPE-HPP, 65% at 1.25 mol % of NR and 26% at 0.35 mol % of NR, respectively. For comparison of the light harvesting activity, we examined the three samples with an equal loading content of NR (0.3 mol %). The η_{ET} values are 58.1, 35.3, and 24.8% for NR@TPE-NCMP-4, NR@TPE-NCMP-2, and NR@TPE-HPP, respectively. Then the data were used to calculate how many TPE units were involved in the energy transfer process. The result reveals that approximately 194 TPE units of TPE-NCMP-4 harvest the photons and funnel the excitation energy to one NR molecule. In contrast, less TPE units in TPE-NCMP-2 (117) and TPE-HPP (83) are effective. This implies that the microporous structure with high surface area is conducive to spatially isolate the dye molecules from one another and independently confine them in the framework to brightly emit upon the energy harvesting and channeling by the TPE-NCMP antenna toward the ultraviolet region. On the contrary, it is unfavorable that a number of NR molecules are filled within a large pore leading to the nonradiation energy yield.

To evaluate the rate constant of energy transfer, we measured the fluorescence lifetimes monitored at 520 nm for TPE-NCMP-4 and NR@TPE-NCMP-4. Figure 3d shows the time-resolved fluorescence decay profiles, both of which have the characteristic of a multiple exponential decay. The average fluorescence times estimated by assuming a quadruple-exponential fitting are 1.57 ns (τ_0) for the TPE-NCMP-4 and 1.21 ns (τ_{DA}) for the NR@TPE-NCMP-4. It is therefore found that the decay of TPE unit emission is reduced by dye doping, again proving the resonance energy transfer without a radiation process. Additionally, the pseudo-first-order rate constant (k_{ET}) of the energy transfer from TPE-NCMP-4 to NR was estimated to be 1.9 × 10^8 s^{-1} using the equation $k_{ET} = 1/\tau_0 - 1/\tau_{DA}$. These results suggest that the energy-transfer process is controlled by rapid exciton diffusion, and such a fast energy transduction is unprecedented for CMP and rarely found for other polymer antennas.[21]

Considering the excellent dispersibility of TPE-NCMPs, NCMP-based films were prepared for use in engineering of light emission devices. Poly(vinyl alcohol) (PVA), which is the commonly used film-forming polymer, can act as binder to agglutinate TPE-NCMPs within the film. The PVA aqueous solution (10 wt %) dispersed a certain amount of phenylboronic acid-modified TPE-NCMPs and the mixture was used to prepare the film on a 96-well plate. A homogeneous and transparent film was obtained after drying at room temperature. For comparison, the bulky TPE-CMP, which was synthesized in toluene without control of size and shape, were insoluble in

dx.doi.org/10.1021/mz5005508 | ACS Macro Lett. 2014, 3, 1139−1144

common solvents and badly suspended in water. Although the PVA was enabled to bond the TPE-CMP powders together, a close look at the prepared film showed the relatively rough surface with the large TPE-CMP grains.

The fluorescence emission of the TPE-NCMP/PVA film could be flexibly tuned by the doping of fluorescent dyes in a wide range of the visible spectrum. The red-emitting dye, Phloxine B (PhB), was doped into the mesostructured TPE-NCMP/PVA film at concentrations of 0.1−0.4 mg/g to the TPE-NCMPs. The broad fluorescence spectrum of TPE-NCMP ranged from λ = 450 to 650 nm and sufficiently overlapped the absorption spectra of the fluorescent dyes; therefore, the efficient excitation energy transfer from TPE units to PhB could be expected. The fluorescence emission spectra of the PhB-doped TPE-NCMP/PVA films are shown in Figure S9 (SI). The green light emission of TPE-NCMP at around 500 nm is gradually quenched with increase of the PhB concentration. Meanwhile, the emission band in the longer wavelength (575−590 nm) region increases gradually. It could be attributed to the fluorescence emission of the doped PhB, indicative of the occurrence of excitation energy transfer from TPE units to PhB. The photographs in Figure 4a display the PhB-doped TPE-NCMP/PVA films without and with irradiation of UV lamp (365 nm). The homogeneous films strongly emit the different colors changing from green to white. As plotted in the CIE 1931 chromaticity diagram (Figure 4b), the emission colors of the PhB-doped TPE-NCMP/PVA films are varied from green with CIE coordinates of (0.26, 0.40) to white (0.31, 0.31) when TPE-NCMPs were doped with 0.1−0.4 mg/g of PhB.

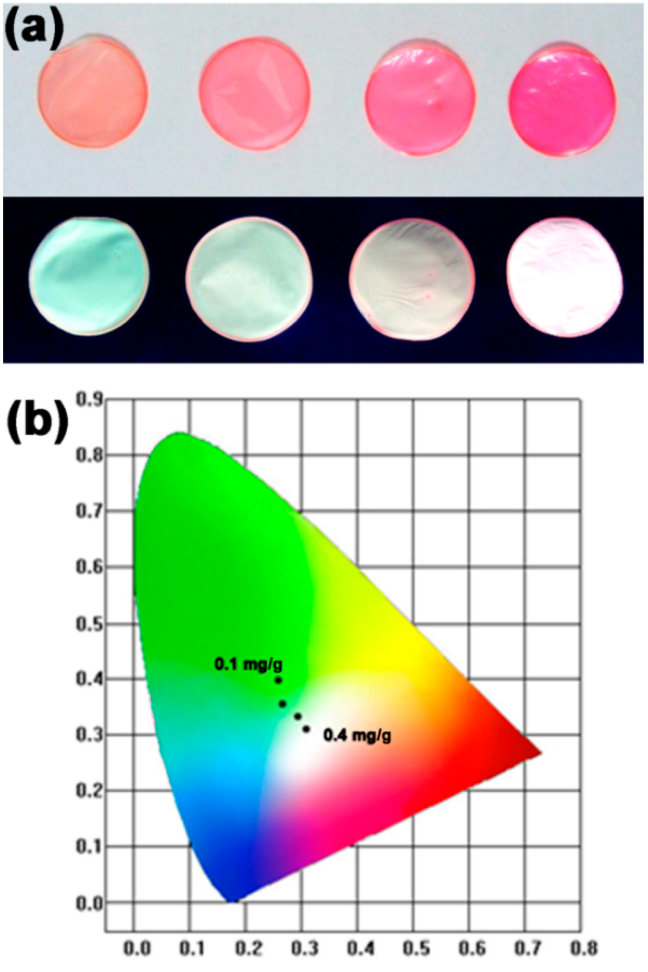

Figure 4. (a) Photographs of casting films without (up) and with (bottom) UV light irradiation. (b) Emission colors in the CIE 1931 chromaticity diagram calculated from the fluorescence emission spectra of PhB@TPE-NCMP/PVA films.

To summarize, a two-step pathway combining miniemulsion and solvothermal techniques was established for exploration of high-quality NCMPs with improved microporosity, dispersible stability, uniform size, and morphology, tunable fluorescence and film-forming characteristic. Also, when TPE units were interwoven into NCMPs by the two-step route, a high quantum yield of AIE fluorescence was observed both in solution and in solid states. Nile Red was entrapped within TEP-NCMPs creating a donor−acceptor couple. The assembled composite was allowed to harvest ultraviolet photons from NCMP skeletons and cooperatively channel the excitation energy of many TPE units to one dye molecule, proving their efficient light harvesting and energy transfer natures. Moreover, blending of TEP-NCMPs with PVA gave a homogeneous film. Phloxine B doping enabled color-tunable photoluminescence over a wide range of the visible spectrum, including a white light emission with CIE coordinates of (0.31, 0.31). Therefore, the developed method is likely to construct versatile NCMPs for the wider applications.

■ ASSOCIATED CONTENT

Supporting Information

Details of materials and methods, SEC spectrum, hydrodynamic diameters, TEM image, N_2 sorption isotherms, pore size distribution, TGA profiles, fluorescence quantum yields, and fluorescence excitation and emission spectra. This material is available free of charge via the Internet at http://pubs.acs.org.

■ AUTHOR INFORMATION

Corresponding Author

*E-mail: guojia@fudan.edu.cn.

Author Contributions

†P.Z. and K.W. contributed equally.

Notes

The authors declare no competing financial interest.

■ ACKNOWLEDGMENTS

We acknowledge the financial support of the NSFC (21004012 and 21474015) and STCSM (13520720200 and 14ZR1402300).

■ REFERENCES

(1) Jiang, J. X.; Su, F.; Trewin, A.; Wood, C. D.; Compbell, N. L.; Niu, H.; Dickinson, C.; Ganin, A. Y.; Rosseinsky, M. J.; Khimyak, Y. Z.; Cooper, A. I. *Angew. Chem., Int. Ed.* **2007**, *46*, 8574−8578.
(2) Jiang, J.; Su, F.; Trewin, A.; Wood, C. D.; Niu, H.; Jones, J. T.; Khimyak, Y. Z.; Cooper, A. I. *J. Am. Chem. Soc.* **2008**, *130*, 7710−7722.
(3) Cooper, A. I. *Adv. Mater.* **2009**, *21*, 1291−1295.
(4) Thomas, A. *Angew. Chem., Int. Ed.* **2010**, *49*, 8328−8344.
(5) Dawson, R.; Cooper, A. I.; Adams, D. J. *Prog. Polym. Sci.* **2012**, *37*, 530−563.
(6) Liu, X.; Xu, Y.; Jiang, D. *J. Am. Chem. Soc.* **2012**, *134*, 8738−8741.
(7) Xu, Y.; Jin, S.; Xu, H.; Nagai, A.; Jiang, D. *Chem. Soc. Rev.* **2013**, *42*, 8012−8031.
(8) Gu, C.; Huang, N.; Gao, J.; Xu, F.; Xu, Y.; Jiang, D. *Angew. Chem., Int. Ed.* **2014**, *53*, 4850−4855.

(9) Bunz, U. H. F.; Seehafer, K.; Geyer, F. L.; Bender, M.; Braun, I.; Smarsly, E.; Freudenberg, J. *Macromol. Rapid Commun.* **2014**, *35*, 1466−1496.
(10) Jiang, J.; Su, F.; Niu, H.; Wood, C. D.; Campbell, N. L.; Khimyak, Y. Z.; Cooper, A. I. *Chem. Commun.* **2008**, 486−488.
(11) Ben, T.; Ren, H.; Ma, S.; Cao, D.; Lan, J.; Jing, X.; Wang, W.; Xu, J.; Deng, F.; Simmons, J. M.; Qiu, S.; Zhu, G. *Angew. Chem., Int. Ed.* **2009**, *48*, 9457−9460.
(12) Li, A.; Wang, L.; Wang, X.; Han, K.; Deng, W. *Angew. Chem., Int. Ed.* **2010**, *49*, 3330−3333.
(13) Chen, Q.; Luo, M.; Wang, T.; Wang, J.; Zhou, D.; Han, Y.; Zhang, C.; Yan, C.; Han, B. *Macromolecules* **2011**, *44*, 5573−5577.
(14) Chen, Q.; Luo, M.; Hammershøj, P.; Zhou, P.; Han, Y.; Laursen, B. W.; Yan, C.; Han, B. *J. Am. Chem. Soc.* **2012**, *134*, 6084−6087.
(15) Liu, X.; Xu, Y.; Guo, Z.; Nagai, A.; Jiang, D. *Chem. Commun.* **2013**, *49*, 3233−3235.
(16) Xiang, Z.; Cao, D. *J. Mater. Chem. A* **2013**, *1*, 2691−2718.
(17) Chen, L.; Yang, Y.; Jiang, D. *J. Am. Chem. Soc.* **2010**, *132*, 9138−9143.
(18) Chen, L.; Yang, Y.; Guo, Z.; Jiang, D. *Adv. Mater.* **2011**, *23*, 3149−3154.
(19) Rose, M. *ChemCatChem* **2014**, *5*, 1166−1182.
(20) Weber, J.; Thomas, A. *J. Am. Chem. Soc.* **2008**, *130*, 6334−6335.
(21) Chen, L.; Honsho, Y.; Seki, S.; Jiang, D. *J. Am. Chem. Soc.* **2010**, *132*, 6742−6748.
(22) Xiang, Z.; Cao, D. *Macromol. Rapid Commun.* **2012**, *33*, 1184−1190.
(23) Feng, X.; Liang, Y.; Zhi, L.; Thomas, A.; Wu, D.; Lieberwirth, I.; Kolb, U.; Müllen, K. *Adv. Funct. Mater.* **2009**, *19*, 2125−2129.
(24) Kou, Y.; Xu, Y.; Guo, Z.; Jiang, D. *Angew. Chem., Int. Ed.* **2011**, *50*, 8753−8757.
(25) Cheng, G.; Hasell, T.; Trewin, A.; Adams, D. J.; Cooper, A. I. *Angew. Chem., Int. Ed.* **2012**, *51*, 12727−12731.
(26) Gu, C.; Chen, Y.; Zhang, Z.; Xue, S.; Sun, S.; Zhang, K.; Zhong, C.; Zhang, H.; Pan, Y.; Lv, Y.; Yang, Y.; Li, F.; Zhang, S.; Huang, F.; Ma, Y. *Adv. Mater.* **2013**, *25*, 3443−3448.
(27) Gu, C.; Chen, Y.; Zhang, Z.; Xue, S.; Sun, S.; Zhong, C.; Zhang, H.; Lv, Y.; Li, F.; Huang, F.; Ma, Y. *Adv. Energy Mater.* **2014**, *4*, DOI: 10.1002/aenm.201301771.
(28) Schwab, M. G.; Crespy, D.; Feng, X.; Landfester, K.; Müllen, K. *Macromol. Rapid Commun.* **2011**, *32*, 1798−1803.
(29) Zhang, P.; Weng, Z.; Guo, J.; Wang, C. *Chem. Mater.* **2011**, *23*, 5243−5249.
(30) Zhang, P.; Guo, J.; Wang, C. *J. Mater. Chem.* **2012**, *22*, 21426−21433.
(31) Wu, K.; Guo, J.; Wang, C. *Chem. Commun.* **2014**, *50*, 695−697.
(32) Hong, Y.; Lam, J. W. Y.; Tang, B. *Chem. Soc. Rev.* **2011**, *40*, 5361−5388.
(33) Wang, Z.; Chen, S.; Lam, J. W. Y.; Qin, W.; Kwok, R. T. K.; Xie, N.; Hu, Q.; Tang, B. *J. Am. Chem. Soc.* **2013**, *135*, 8238−8245.
(34) Xu, Y.; Chen, L.; Cuo, Z.; Nagai, A.; Jiang, D. *J. Am. Chem. Soc.* **2011**, *133*, 17622−17625.